Supplemental Material to

Connecting Rodent and Human Pharmacokinetic Models for the Design and Translation of Glucose-Responsive Insulin

Jing Fan Yang[1], Xun Gong[1], Naveed A. Bakh[1], Kelley Carr[2], Nelson F. B. Phillips[2], Faramarz Ismail-Beigi[2], Michael A. Weiss[3], and Michael S. Strano[1]

[1]Department of Chemical Engineering, Massachusetts Institute of Technology, MA 02139, USA.
[2]Department of Biochemistry, Case Western Reserve University, OH 44106, USA.
[3]Department of Biochemistry and Molecular Biology, Indiana University School of Medicine, IN 46202, USA.

Correspondence author: Michael S. Strano, strano@mit.edu

S1. Animal Preparation, Care, and Data Collection

As said, blood glucose time trajectories were collected from normal and diabetic rats for parameter estimation. Male Lewis rats weighing 250 to 300 grams were obtained from Envigo. Rats to be rendered diabetic were injected intraperitoneally with 48 mg/kg streptozotocin (STZ; from MP Biomedicals). Diabetes was confirmed after a 72-hour quarantine by blood glucose measurement of > 250 mg/dL. A second injection of 48 mg/kg STZ was given if rats did not become diabetic after the first injection. Rats were repeatedly used in experiments after two or more weeks of rest period, and were used in experiments no longer than one year post stable induction of diabetes. For insulin studies, food was removed prior to the start of the experiment. The rats were weighed and the tip of the tail was snipped with a razor blade and milked for a small blood sample in which blood glucose levels were measured with standard glucometers (EasyMax V). Insulin lispro was injected subcutaneously in diabetic or normal (non-diabetic) rats. A time course of the insulin's action profile was created.

S2. Mathematical Model Setup

In each organ *k*, the concentration of a solute *s* is governed by:

$$V^s_{k,\mathrm{v}}\frac{d[s]_{k,\mathrm{v}}}{dt} = Q^s_k([s]_{\mathrm{heart}} - [s]_{k,\mathrm{v}}) - \frac{V^s_{k,\mathrm{i}}}{T^s_k}([s]_{k,\mathrm{v}} - [s]_{k,\mathrm{i}}) + R^s_{k,\mathrm{v,prod/uptake}} + V^{\mathrm{I}}_{k,\mathrm{v}}\nu_s r_{\mathrm{GRI}} \tag{S1}$$

$$V^s_{k,\mathrm{i}}\frac{d[s]_{k,\mathrm{i}}}{dt} = \frac{V^s_{k,\mathrm{i}}}{T^s_k}([s]_{k,\mathrm{v}} - [s]_{k,\mathrm{i}}) + R^s_{k,\mathrm{i,prod/uptake}} + V^{\mathrm{I}}_{k,\mathrm{i}}\nu_s r_{\mathrm{GRI}} \tag{S2}$$

$$r_{\mathrm{GRI}} = k_f[\mathrm{G}]_k[\mathrm{D}]_k - k_r[\mathrm{I}]_k \tag{S3}$$

Where subscripts c and i denote vascular and interstitial (if applicable) volumes respectively, the transcapillary diffusion between which captured by T^s_k. The compartmental volumes and blood flow rates, denoted V^s_k and Q^s_k respectively, are based on anatomical measurements of rodents listed in Table S1. We

simulate the actions of freely circulating GRIs in this report, for which the stoichiometric coefficients (v) are -1, +1, -1, and 0 for the four solutes – glucose, insulin, dormant GRI, and glucagon – respectively. PAMERAH inherits the pancreatic insulin release as well as the oral dosing models from Bisker *et al.* (S1) and follows the initialization protocol outlined in Bakh *et al.* (S2) Parameters pertaining to insulin release are adapted to rodents based on Sorensen (S3).

We further clarify, with the following short tutorial, how the concise general governing equations above generate a large network of differential equations needed for simulation. We take the adipose peripheral compartments as an example. Within each compartment, the rate of change in glucose level $V^{\mathrm{G}}_{\mathrm{adipose,v/i}}\, d[\mathrm{G}]_{\mathrm{adipose,v/i}}/dt$ equals rate of exchange with other organs summed with the glucose production/consumption rate within the compartment itself. For the adipose vascular compartment, the former encompasses incoming glucose carried from heart by blood flow ($Q^{\mathrm{G}}_{\mathrm{adipose}}[\mathrm{G}]_{\mathrm{heart}}$), the outgoing glucose circulated back ($-Q^{\mathrm{G}}_{\mathrm{adipose}}[\mathrm{G}]_{\mathrm{adipose,v}}$, with the negative sign denoting that glucose exits the system), and the exchange with the interstitial compartment ($-(V^{\mathrm{G}}_{\mathrm{adipose,i}}/T^{\mathrm{G}}_{\mathrm{adipose}})([\mathrm{G}]_{\mathrm{adipose,v}}-[\mathrm{G}]_{\mathrm{adipose,i}})$). Inside the compartment, glucose reacts with dormant GRI and is consumed. Its rate is governed by the overall reaction rate $r_{\mathrm{GRI}} = k_f[\mathrm{G}]_{\mathrm{adipose}}[\mathrm{D}]_{\mathrm{adipose}} - k_r[\mathrm{I}]_{\mathrm{adipose}}$. This rate has to be corrected by the stoichiometric coefficient $\nu_{\mathrm{G}} = -1$, which states that one unit of glucose is consumed for each unit of reaction $\mathrm{G} + \mathrm{D} \rightleftharpoons \mathrm{I}$. The governing ODE for the adipose vascular compartment is then (*cf.* Equation S1):

$$\underbrace{V^{\mathrm{G}}_{\mathrm{adipose,v}}\frac{d[\mathrm{G}]_{\mathrm{adipose,v}}}{dt}}_{\text{rate of change in the compartment}} = \underbrace{Q^{\mathrm{G}}_{\mathrm{adipose}}([\mathrm{G}]_{\mathrm{heart}}-[\mathrm{G}]_{\mathrm{adipose,v}})}_{\text{inflow/outflow term}} \underbrace{-\frac{V^{\mathrm{G}}_{\mathrm{adipose,i}}}{T^{\mathrm{G}}_{\mathrm{adipose}}}([\mathrm{G}]_{\mathrm{adipose,v}}-[\mathrm{G}]_{\mathrm{adipose,i}})}_{\text{transcapillary exchange term}} \underbrace{-V^{\mathrm{I}}_{\mathrm{adipose,v}}r_{\mathrm{GRI,v}}}_{\text{GRI kinetics term}} \tag{S4}$$

On the other hand, the interstitial space is not connected to any external organ (Figure 1), which allows us to drop the inflow/outflow terms ($Q[\mathrm{G}]$). In addition, glucose is taken up by the adipose tissues at a rate $R_{\mathrm{adipose\ PGU}}$ modulated by the local glucose and hormone concentrations (Table S2), where PGU stands for peripheral glucose uptake. The governing ODE for the adipose interstitial space is therefore:

$$\underbrace{V^{\mathrm{G}}_{\mathrm{adipose,i}}\frac{d[\mathrm{G}]_{\mathrm{adipose,i}}}{dt}}_{\text{rate of change in the compartment}} = \underbrace{\frac{V^{\mathrm{G}}_{\mathrm{adipose,i}}}{T^{\mathrm{G}}_{\mathrm{adipose}}}([\mathrm{G}]_{\mathrm{adipose,v}}-[\mathrm{G}]_{\mathrm{adipose,i}})}_{\text{transcapillary exchange term}} \underbrace{-R_{\mathrm{adipose\ PGU}}}_{\text{local prod/uptake term}} \underbrace{-V^{\mathrm{I}}_{\mathrm{adipose,i}}r_{\mathrm{GRI,i}}}_{\text{GRI kinetics term}} \tag{S5}$$

which is exactly Equation S2 specific to the adipose tissues. Note that the transcapillary exchange term changes sign.

By the same method, we write the ODEs for active insulin in adipose compartments:

$$V^{\mathrm{I}}_{\mathrm{adipose,v}}\frac{d[\mathrm{I}]_{\mathrm{adipose,v}}}{dt} = Q^{\mathrm{I}}_{\mathrm{adipose}}([\mathrm{I}]_{\mathrm{heart}}\text{-}[\mathrm{I}]_{\mathrm{adipose,v}}) - \frac{V^{\mathrm{I}}_{\mathrm{adipose,i}}}{T^{\mathrm{I}}_{\mathrm{adipose}}}([\mathrm{I}]_{\mathrm{adipose,v}}-[\mathrm{I}]_{\mathrm{adipose,i}}) + V^{\mathrm{I}}_{\mathrm{adipose,v}}r_{\mathrm{GRI,v}} \tag{S6}$$

$$V^{\mathrm{I}}_{\mathrm{adipose,i}}\frac{d[\mathrm{I}]_{\mathrm{adipose,i}}}{dt} = \frac{V^{\mathrm{I}}_{\mathrm{adipose,i}}}{T^{\mathrm{I}}_{\mathrm{adipose}}}([\mathrm{I}]_{\mathrm{adipose,v}}-[\mathrm{I}]_{\mathrm{adipose,i}}) - R_{\mathrm{AIC}} + V^{\mathrm{I}}_{\mathrm{adipose,i}}r_{\mathrm{GRI,i}} \tag{S7}$$

where R_{AIC} is the rate of adipose insulin clearance (Table S2). Note that the GRI kinetics terms change sign as compared to Equations S4 and S5 since the stoichiometric coefficient $\nu_{\mathrm{I}} = +1$ for insulin: each unit of

GRI reaction produces one unit of insulin. With the steps outlined in this tutorial, ODEs for other compartments and for other solutes can be generated likewise from Equations S1 and S2.

The rates of production/consumption of *s*, $R^{s}_{k,\text{prod/uptake}}$, are detailed below in Table S2 together with insulin absorption and clearance rates. Since the steady-state metabolism in rodents is not systematically characterized or published, its associated variables are estimated from experimental data. A number of multipliers, which characterize organs' responsiveness to hormonal regulations, are selected by sensitivity analyses (SA) and estimated. The same applies to the unknown insulin clearance fractions and transcapillary diffusion times (Figure S1). The latter turn out to carry insignificant impacts and are hence simply scaled by body mass (Table S1). For the PAMERAH ordinary differential equation system we concern, the parametric sensitivity of the blood glucose concentration on parameter p_j is defined as:

$$Z_j = \int_0^{360\,\text{min}} \sum_{\text{health}} \sum_{\text{doses}} \frac{[\text{G}]_{\text{heart}}}{p_j} \frac{dp_j}{d[\text{G}]_{\text{heart}}} dt \tag{S8}$$

consistent with prior applications of SA (S4,S5). As said, only the numerically sensitive variables, marked in Figure S1, are subject to parametric estimation to avoid overfitting. The sets of estimated parameters are almost identical for the two rodents except $M^{\Gamma 0}_{\text{HGP}}$, which is impactful only in mice. The SA results in Figure S1 are obtained with the finalized parameter values as the basis.

Table S1. Physiological parameters for rats and mice based on *a priori* animal anatomical measurements.

	Physiological Parameter	Rats	Mice	Unit	Physiological Parameter	Rats	Mice	Unit
Volumes of Compartments[a]	$V^{\text{G}}_{\text{brain,v}}$	2.44E-03	1.69E-04	[dL]	$V^{\text{I}}_{\text{brain}}$	1.86E-04	1.21E-05	[L]
	$V^{\text{G}}_{\text{brain,i}}$	3.41E-03	1.07E-03					
	$V^{\text{G}}_{\text{heart}}$	4.89E-02	5.79E-03		$V^{\text{I}}_{\text{heart}}$	3.74E-03	4.14E-04	
	$V^{\text{G}}_{\text{lungs}}$	8.03E-02	1.78E-02		$V^{\text{I}}_{\text{lungs}}$	3.20E-03	6.86E-04	
	$V^{\text{G}}_{\text{gut}}$	2.97E-02	8.26E-03		$V^{\text{I}}_{\text{gut}}$	2.62E-03	7.43E-04	
	$V^{\text{G}}_{\text{kidneys}}$	1.90E-02	2.93E-03		$V^{\text{I}}_{\text{kidneys}}$	1.55E-03	2.43E-04	
	$V^{\text{G}}_{\text{periphery,v}}$	6.54E-02	5.20E-03		$V^{\text{I}}_{\text{periphery,v}}$	5.00E-03	3.72E-04	
	$V^{\text{G}}_{\text{periphery,i}}$	2.96E-01	1.62E-02		$V^{\text{I}}_{\text{periphery,i}}$	2.96E-02	1.62E-03	
Blood Flow Rates[b]	$Q^{\text{G}}_{\text{brain}}$	2.44E-02	8.88E-04	[dL/min]	$Q^{\text{I}}_{\text{brain}}$	1.86E-03	6.35E-05	[L/min]
	$Q^{\text{G}}_{\text{heart}}$	2.21E-01	5.12E-02		$Q^{\text{I}}_{\text{heart}}$	6.75E-02	3.66E-03	
	$Q^{\text{G}}_{\text{lungs}}$	1.61E-01	1.73E-02		$Q^{\text{I}}_{\text{lungs}}$	1.23E-02	1.24E-03	
	$Q^{\text{G}}_{\text{gut}}$	1.46E-01	1.47E-02		$Q^{\text{I}}_{\text{gut}}$	1.11E-02	1.05E-03	
	$Q^{\text{G}}_{\text{kidney}}$	1.46E-01	9.21E-03		$Q^{\text{I}}_{\text{kidney}}$	1.12E-02	6.59E-04	
	$Q^{\text{G}}_{\text{periphery}}$	5.51E-01	2.38E-02		$Q^{\text{I}}_{\text{periphery}}$	4.21E-02	1.70E-03	
	$Q^{\text{G}}_{\text{hepatic artery}}$	1.56E-02	2.66E-03		$Q^{\text{I}}_{\text{hepatic artery}}$	1.19E-03	1.91E-04	
	$Q_{\text{muscle}} / Q_{\text{adipose}}$	2.18E+00	2.74E+00	[-]				

TDT[c]	$T^{G}_{periphery}$	1.32E-01	2.52E-2	[min]	$T^{I}_{periphery}$	5.28E-01	1.01E-1	[min]
	T^{G}_{brain}	5.54E-02	1.06E-2					

[a] Compartmental volumes are based on measurements in Brown *et al.*, Thurlby and Trayhurn, and Peters (S6–S8).

[b] Blood flow rates are based on measurements in Ishise *et al.*, Wang *et al.*, Brown *et al.*, and Thurlby and Trayhurn (S6,S7,S9,S10).

[c] TDT, transcapillary diffusion time between the vascular and interstitial volumes. They are scaled by body mass from the human models (S1,S2). They are not estimated from experimental data given their low sensitivities in both mice and rats (Figure S1).

Table S2. Pharmacokinetic parameters for rats and mice. Estimated (*Est.*) and distinguishingly parameterized (*Dis.*; *i.e.* separately estimated for the healthy and diabetic populations) variables are marked by circles.

RATS			Healthy	Diabetic	Unit	Est.	Dis.
Hepatic Glucose Uptake	R_{HGU}	=	$R^{basal}_{HGU} M^{G}_{HGU} M^{I}_{HGU}$		[mg/min]		
	R^{basal}_{HGU}	=	4.01E+00	3.02E+00	[mg/min]	○[a]	○
	M^{G}_{HGU}	=	$2.37 + 1.67\tanh\{2.44([G]_{L,n} - 1.48)\}$		[-]	○[b]	
	$\frac{dM^{I}_{HGU}}{dt}$	=	$(M^{I\infty}_{HGU} - M^{I}_{HGU}) / \tau_1$		[min^{-1}]		
	$M^{I\infty}_{HGU}$	=	$2.00\tanh(0.55[I]_{L,n})$		[-]		
	τ_1	=	7.10E-03		[min]	○	
Hepatic Glucose Production	R_{HGP}	=	$R^{basal}_{HGP} M^{G}_{HGP} M^{I}_{HGP} M^{\Gamma}_{HGP}$		[mg/min]		
	R^{basal}_{HGP}	=	$\sum_{k=H, P, B, RBC, G} R^{basal}_{kGU}$		[mg/min]		
	M^{G}_{HGP}	=	$1.42 - 1.41\tanh\{0.62([G]_{L,n} - 0.50)\}$	$2.15 - 1.41\tanh\{2.30([G]_{L,n} - 0.50)\}$	[-]	○[b]	○
	$\frac{dM^{I}_{HGP}}{dt}$	=	$(M^{I\infty}_{HGP} - M^{I}_{HGP}) / \tau_1$		[min^{-1}]		
	$M^{I\infty}_{HGP}$	=	$1.16 - 0.16\tanh\{79.79([I]_{L,n} - 0.0003)\}$		[-]	○	
	M^{Γ}_{HGP}	=	$M^{\Gamma 0}_{HGP} - f_2$		[-]		
	$M^{\Gamma 0}_{HGP}$	=	$2.70\tanh\{0.39[\Gamma]_n\}$		[-]		
	df_2 / dt	=	$\{(M^{\Gamma 0}_{HGP} - 1) / 2 - f_2\} / \tau_2$		[min^{-1}]		
	τ_2	=	1.00E-02		[min]	○	
Periphery Glucose Uptake	R_{PGU}	=	$R^{basal}_{PGU} M^{G}_{PGU} M^{I}_{PGU}$		[mg/min]		
	R^{basal}_{PGU}	=	1.02E+00	1.67E+00	[mg/min]	○[a]	○
	M^{G}_{PGU}	=	$[G]_{periphery,i,n}$		[-]		
	M^{I}_{PGU}	=	$7.03 + 6.52\tanh\{0.34([I]_{periphery,i,n} - 5.82)\}$		[-]		
Kidney Glucose Excretion[c]	R_{KGE}	=	$\begin{cases} 0.50 + 0.50\tanh[0.0081([G]_{kidney} - 584.77)] \\ \text{if } 0 \le [G]_{kidney} < 584.77\ \text{mg dL}^{-1} \\ -330 + 0.564[G]_{kidney} \\ \text{if } [G]_{kidney} > 584.77\ \text{mg dL}^{-1} \end{cases}$		[mg/min]		
Kidney Insulin Clearance	R_{KIC}	=	$F_{KIC} Q^{I}_{K} I_K$		[mU/min]		
	F_{KIC}	=	3.00E-01		[-]		
Liver Insulin Clearance	R_{LIC}	=	$F_{LIC}(Q^{I}_{adipose}[I]_{heart} + Q^{I}_{gut}[I]_{gut})$		[mU/min]		
	F_{LIC}	=	4.00E-01		[-]		

SUPPLEMENTARY DATA

Muscle Insulin Clearance	R_{MIC}	=	$\dfrac{[\mathrm{I}]_{\mathrm{muscle,i}}}{\dfrac{1-F_{PIC}}{F_{PIC}}\dfrac{1}{Q^{\mathrm{I}}_{\mathrm{muscle}}}-\dfrac{T^{\mathrm{I}}_{\mathrm{muscle}}}{V^{\mathrm{I}}_{\mathrm{muscle,i}}}}$		[mU/min]		
	F_{PIC}	=	1.13E-02	4.90E-01	[-]	○	○
Adipose Insulin Clearance	R_{AIC}	=	$\dfrac{[\mathrm{I}]_{\mathrm{adipose,i}}}{\dfrac{1-F_{PIC}}{F_{PIC}}\dfrac{1}{Q^{\mathrm{I}}_{\mathrm{adipose}}}-\dfrac{T^{\mathrm{I}}_{\mathrm{adipose}}}{V^{\mathrm{I}}_{\mathrm{adipose,i}}}}$		[mU/min]		
Brain Glucose Uptake	R_{BGU}	=	1.59E+00	3.36E+00	[mg/min]	○[a]	○
Red Blood Cell Glucose Uptake	R_{RBCU}	=	7.36E-01	1.59E+00	[mg/min]	○[a]	○
Gut Glucose Uptake	R_{GGU}	=	3.50E+00	3.15E+00	[mg/min]	○[a]	○
Subcutaneous Insulin Absorption[d]	$R_{\mathrm{SIA,adipose,i}}$	=	$k_{\mathrm{abs}}[\mathrm{I_{dm}}]_{\mathrm{depot}}$		[mU/L/min]		
	$\dfrac{d[\mathrm{I_{dm}}]}{dt}$	=	$k_{\mathrm{h/dm}}[\mathrm{I_{hex}}]-(k_{\mathrm{abs}}+k_{\mathrm{loss}})[\mathrm{I_{dm}}]$		[mU/L/min]		
	$\dfrac{d[\mathrm{I_{hex}}]}{dt}$	=	$-(k_{\mathrm{h/dm}}+k_{\mathrm{loss}})[\mathrm{I_{hex}}]$		[mU/L/min]		
	k_{abs}	=	1.30E-02	6.70E-03	[min^{-1}]	○	○
	$k_{\mathrm{h/dm}}$	=	1.22E-02		[min^{-1}]	○	
	k_{loss}	=	$3D_{\mathrm{inj}}(3V_{\mathrm{inj}}/4\pi)^{-2/3}$		[min^{-1}]		
	D_{inj}	=	9.00E-5		[cm^2/min]		

MICE							
			Healthy	Diabetic	Unit		
Hepatic Glucose Uptake	R_{HGU}	=	$R^{\mathrm{basal}}_{\mathrm{HGU}}M^{\mathrm{G}}_{\mathrm{HGU}}M^{\mathrm{I}}_{\mathrm{HGU}}$		[mg/min]		
	$R^{\mathrm{basal}}_{\mathrm{HGU}}$	=	1.64E-02	1.37E-02	[mg/min]	○[e]	○
	$M^{\mathrm{G}}_{\mathrm{HGU}}$	=	$5.66 + 5.66\tanh\{2.44([\mathrm{G}]_{\mathrm{L,n}} - 1.48)\}$		[-]	○[b]	
	$\dfrac{dM^{\mathrm{I}}_{\mathrm{HGU}}}{dt}$	=	$(M^{\mathrm{I}\infty}_{\mathrm{HGU}} - M^{\mathrm{I}}_{\mathrm{HGU}})/\tau_1$		[min^{-1}]		
	$M^{\mathrm{I}\infty}_{\mathrm{HGU}}$	=	$2.00\tanh(0.55[\mathrm{I}]_{\mathrm{L,n}})$		[-]		
	τ_1	=	2.00E-03		[min]	○	
Hepatic Glucose Production	R_{HGP}	=	$R^{\mathrm{basal}}_{\mathrm{HGP}}M^{\mathrm{G}}_{\mathrm{HGP}}M^{\mathrm{I}}_{\mathrm{HGP}}M^{\Gamma}_{\mathrm{HGP}}$		[mg/min]		
	$R^{\mathrm{basal}}_{\mathrm{HGP}}$	=	$\sum_{k=\mathrm{H,\ P,\ B,\ RBC,\ G}} R^{\mathrm{basal}}_{k\mathrm{GU}}$		[mg/min]		
	$M^{\mathrm{G}}_{\mathrm{HGP}}$	=	$1.06 - 6.39\tanh\{0.02([\mathrm{G}]_{\mathrm{L,n}} - 0.50)\}$	$1.40 - 6.39\tanh\{0.13([\mathrm{G}]_{\mathrm{L,n}} - 0.50)\}$	[-]	○[b]	○
	$\dfrac{dM^{\mathrm{I}}_{\mathrm{HGP}}}{dt}$	=	$R^{\mathrm{basal}}_{\mathrm{HGP}}M^{\mathrm{G}}_{\mathrm{HGP}}M^{\mathrm{I}}_{\mathrm{HGP}}M^{\Gamma}_{\mathrm{HGP}}$		[min^{-1}]		
	$M^{\mathrm{I}\infty}_{\mathrm{HGP}}$	=	$0.90 - 0.13\tanh\{1.67([\mathrm{I}]_{\mathrm{L,n}} - 1.56)\}$	$-5.25 - 8.49\tanh\{1.67([\mathrm{I}]_{\mathrm{L,n}} - 1.56)\}$	[-]	○[b]	○
	$M^{\Gamma}_{\mathrm{HGP}}$	=	$M^{\Gamma 0}_{\mathrm{HGP}} - f_2$		[-]		
	$M^{\Gamma 0}_{\mathrm{HGP}}$	=	$1.00\tanh\{3.91[\Gamma]_{\mathrm{n}}\}$		[-]	○[b]	
	df_2/dt	=	$\{(M^{\Gamma 0}_{\mathrm{HGP}} - 1)/2 - f_2\}/\tau_2$		[min^{-1}]		
	τ_2	=	7.50E-03		[min]	○	
Periphery Glucose Uptake	R_{PGU}	=	$R^{\mathrm{basal}}_{\mathrm{PGU}}M^{\mathrm{G}}_{\mathrm{PGU}}M^{\mathrm{I}}_{\mathrm{PGU}}$		[mg/min]		
	$R^{\mathrm{basal}}_{\mathrm{PGU}}$	=	3.33E-02	2.48E-02	[mg/min]	○[e]	○
	$M^{\mathrm{G}}_{\mathrm{PGU}}$	=	$[\mathrm{G}]_{\mathrm{periphery,i,n}}$		[-]		

	$M^{\mathrm{I}}_{\mathrm{PGU}}$	=	$7.03 + 6.52\tanh\{0.34([\mathrm{I}]_{\mathrm{periphery,i,n}} - 5.82)\}$		[-]		
Kidney Glucose Excretion[c]	R_{KGE}	=	$\begin{cases} 0.50 + 0.50\tanh[0.0081([\mathrm{G}]_{\mathrm{kidney}} - 584.77)] \\ \quad \text{if } 0 \le [\mathrm{G}]_{\mathrm{kidney}} < 584.77\,\mathrm{mg\,dL^{-1}} \\ -330 + 0.564[\mathrm{G}]_{\mathrm{kidney}} \\ \quad \text{if } [\mathrm{G}]_{\mathrm{kidney}} > 584.77\,\mathrm{mg\,dL^{-1}} \end{cases}$		[mg/min]		
Kidney Insulin Clearance	R_{KIC}	=	$F_{KIC} Q^{I}_{K} I_{K}$		[mU/min]		
	F_{KIC}	=	3.00E-01		[-]		
Liver Insulin Clearance	R_{LIC}	=	$F_{LIC}(Q^{\mathrm{I}}_{\mathrm{adipose}}[\mathrm{I}]_{\mathrm{heart}} + Q^{\mathrm{I}}_{\mathrm{gut}}[\mathrm{I}]_{\mathrm{gut}})$		[mU/min]		
	F_{LIC}	=	4.00E-01		[-]		
Muscle Insulin Clearance	R_{MIC}	=	$\dfrac{[\mathrm{I}]_{\mathrm{muscle,i}}}{\dfrac{1-F_{PIC}}{F_{PIC}}\dfrac{1}{Q^{\mathrm{I}}_{\mathrm{muscle}}} - \dfrac{T^{\mathrm{I}}_{\mathrm{muscle}}}{V^{\mathrm{I}}_{\mathrm{muscle,i}}}}$		[mU/min]		
	F_{PIC}	=	1.50E-01	9.00E-01	[-]	○	○
Adipose Insulin Clearance	R_{AIC}	=	$\dfrac{[\mathrm{I}]_{\mathrm{adipose,i}}}{\dfrac{1-F_{PIC}}{F_{PIC}}\dfrac{1}{Q^{\mathrm{I}}_{\mathrm{adipose}}} - \dfrac{T^{\mathrm{I}}_{\mathrm{adipose}}}{V^{\mathrm{I}}_{\mathrm{adipose,i}}}}$		[mU/min]		
Brain Glucose Uptake	R_{BGU}	=	8.60E-03	1.71E-02	[mg/min]	○[e]	○
Red Blood Cell Glucose Uptake	R_{RBCU}	=	8.70E-03	9.00E-03	[mg/min]	○[e]	○
Gut Glucose Uptake	R_{GGU}	=	1.21E-02	1.21E-02	[mg/min]	○[e]	○
Subcutaneous Insulin Absorption[d]	$R_{\mathrm{SIA,adipose,i}}$	=	$k_{\mathrm{abs}}[\mathrm{I_{dm}}]_{\mathrm{depot}}$		[mU/L/min]		
	$\dfrac{d[\mathrm{I_{dm}}]}{dt}$	=	$k_{\mathrm{h/dm}}[\mathrm{I_{hex}}] - (k_{\mathrm{abs}} + k_{\mathrm{loss}})[\mathrm{I_{dm}}]$		[mU/L/min]		
	$\dfrac{d[\mathrm{I_{hex}}]}{dt}$	=	$-(k_{\mathrm{h/dm}} + k_{\mathrm{loss}})[\mathrm{I_{hex}}]$		[mU/L/min]		
	k_{abs}	=	2.28E-02	7.70E-03	[min^{-1}]	○	○
	$k_{\mathrm{h/dm}}$	=	5.65E-02		[min^{-1}]		
	k_{loss}	=	$3D_{\mathrm{inj}}(3V_{\mathrm{inj}}/4\pi)^{-2/3}$		[min^{-1}]		
	D_{inj}	=	9.00E-5		[cm^2/min]		

[a] Base steady-state metabolic rates of rats are estimated from literature-based initial guesses (S11–S14).

[b] Note that the adaptation of transfer functions has only one degree of freedom for each. That is, only one parameter in each transfer function is estimated. $[\mathrm{G}]_{k,\mathrm{n}}$ and $[\mathrm{I}]_{k,\mathrm{n}}$ denotes glucose and insulin concentrations in compartment k normalized by the steady state levels. $[\Gamma]_{\mathrm{n}}$ in turn represents the normalized glucagon concentration. All multipliers (Ms) should assume a value of 1 for a normalized concentration of 1.

[c] The kidney glucose excretion rate as a function of glucose concentration is based on data published by Robson *et al*. (S15)

[d] Simulation of the subcutaneous injection depot follows the work by Bakh *et al.* (S2), who adopted a model originally designed and validated by Wong *et al.* (S16,S17) for regular insulin. Among the states whose dynamic equilibrium dictates the subcutaneous absorption kinetics, dimeric and monomeric insulins are absorbed much faster than the hexameric state ($\mathrm{I_{hex}}$). Wong and colleagues therefore lumped the former two together into the term $\mathrm{I_{dm}}$, formed from the dissociation of hexamers with a rate constant $k_{\mathrm{h/dm}}$. The dimers/monomers are then absorbed from the injection depot into the main circulation at a rate characterized by k_{abs}. Meanwhile, both states suffer from some diffusive loss described by the rate constant k_{loss}, computed from the injection volume V_{inj} and the insulin diffusivity D_{inj}. Numerical value for the latter is obtained from Vogel (S18). Readers may substitute the injection depot for other subcutaneous absorption models as well, such as that by Tarín *et al.* which assumed only a hexamer-dimer equilibrium (S19).

[e] Base steady-state metabolic rates of mice are estimated from literature-based initial guesses (S20–S23).

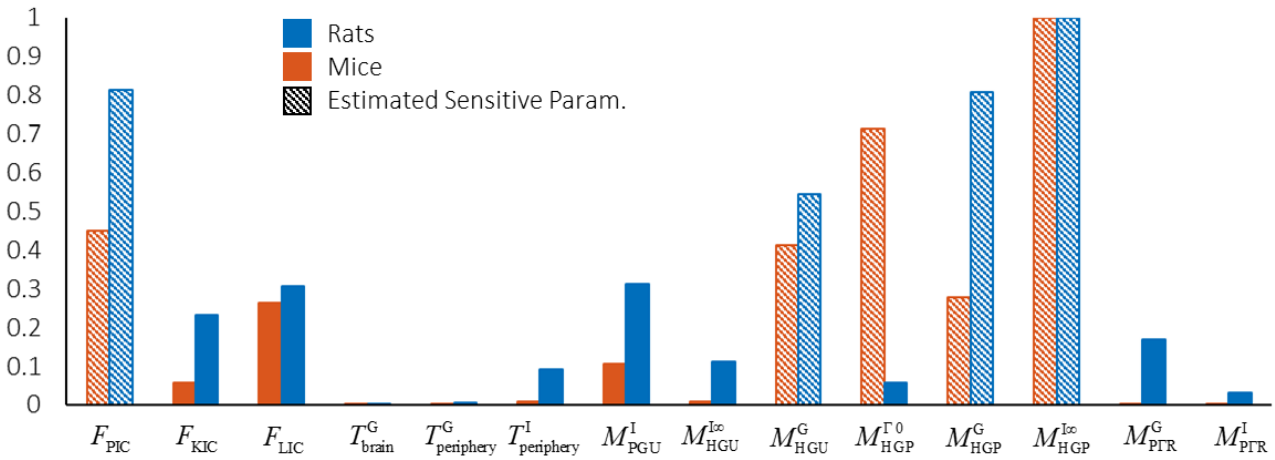

Figure S1. Sensitivities of insulin clearance fractions, transcapillary diffusion time constants, and multipliers for rats (blue) and mice (red). Only the highly sensitive, or impactful, variables are selected for parametric estimation (hatched bars). As the blood glucose level is relatively insensitive to murine transcapillary diffusion times, the latter are simply approximated via body mass scaling (Table S1). Note that the sensitivity analyses presented in this figure assume the finalized parameter values as the bases.

S3. Extension to a Complex GRI: MK-2640

The modularity of PAMERAH offers a good degree of modeling flexibility, allowing the approach to be extended to other GRI mechanisms as well. One may replace the simple GRI kinetics $G + D \rightleftharpoons I$ with a set of equations describing the appropriate glucose-responsive action, and "plug" them back to the compartmental model of physiology. We have demonstrated in the main text that such mathematical representations of glucose-responsiveness apply well to freely circulating GRIs of the simplest kinetics. In this section, we show that more complex mechanisms involving endogenous proteins are no exceptions – by outlining how MK-2640 will be modeled. Merck's MK-2640, the only GRI studied clinically to this date, performed much less convincingly in humans than in preclinical models (S24). The failed translation prompts us to wonder if PAMERAH could have helped.

While the freely circulating GRIs "activate" the insulin component triggered by glucose binding, MK-2640 is intrinsically potent for countering hyperglycemia. The responsiveness lies in its glucose-dependent clearance by mannose receptor C-type 1 (MR), a strategy first explored by Zion and Lancaster (S25). Given the dual affinity to MR and the insulin receptor (IR), the potency of MK-2640 is therefore determined by its partitioning, which, as illustrated in Figure S2, is modulated by glucose competing for MR binding sites. Under hyperglycemic conditions, strong competition from glucose shifts MK-2640's partition towards IR binding, thereby lowering the blood glucose level. Conversely, a larger portion of the GRI is cleared by MR under hypoglycemia, which effectively reduces the drug's availability to IR, and hence the potency (S26,S27).

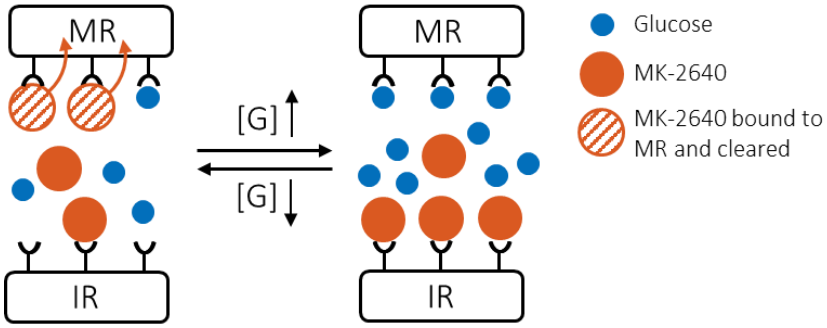

Figure S2. Glucose-responsive mechanism of MK-2640. The mannosylated insulin analogs (red) bind to both the insulin receptor (IR) and mannose receptor (MR), with the latter providing an additional route for GRI clearance and hence a reduction of its availability to IR. As the MR binding activity is engineered to compete with glucose (blue), a higher (lower) local glucose concentration in turn decreases (enhances) MK-2640's MR-mediated clearance. As a result, more glucose-lowering MK-2640 is made available to IR under hyperglycemia and *vice versa*.

As said, GRI mechanisms involving endogenous proteins, though arguably more complex, can be modeled as a set of chemical reactions. Similar techniques have been applied to modeling surface adsorption (*e.g.* the Langmuir isotherm) and enzyme kinetics (*e.g.* the Michaelis-Menten equation) (S28,S29). As a matter of fact, the kinetics of competitive enzyme inhibition (S30) is very much analogous to the action of MK-2640. We therefore propose the following kinetics for the latter:

$$\theta + [\mathrm{GRI}] \underset{k_{-1}}{\overset{k_1}{\rightleftharpoons}} \theta_{\mathrm{GRI}} \xrightarrow{k_2} \theta \tag{S9}$$

$$\theta + h[\mathrm{G}] \underset{k_{-3}}{\overset{k_3}{\rightleftharpoons}} \theta_{\mathrm{G}} \tag{S10}$$

where θ, θ_{G}, and θ_{GRI} stand for concentrations of empty MR binding sites, those bound to glucose, and those to MK-2640. [G] and [GRI] are the local concentrations of glucose and MK-2640. Evidently, Equations S9 and S10 respectively describe the binding of MK-2640 and glucose to MR. After the GRI is internalized and cleared, the binding site is regenerated to the protein surface. Considering that binding of an inhibitor (glucose) is often cooperative in practice (S31), we introduce to Equation S10 the Hill coefficient h, a common indicator in biochemistry for the degree of cooperativity (S32). Do note that as we will see, not all reaction rate constants need to be explicitly provided. Under the quasi-steady-state assumption and acknowledging that $\theta_{\mathrm{GRI}} \xrightarrow{k_2} \theta$ is the rate-limiting step, we arrive at:

$$\left.\begin{aligned} \frac{d\theta_{\mathrm{GRI}}}{dt} = 0 \Rightarrow \theta_{\mathrm{GRI}} &= \frac{[\mathrm{GRI}]\theta}{K_m} \\ \frac{d\theta_{\mathrm{G}}}{dt} = 0 \Rightarrow \theta_{\mathrm{G}} &= K_{\mathrm{G}}[\mathrm{G}]^h\theta \\ \theta + \theta_{\mathrm{GRI}} + \theta_{\mathrm{G}} &= \theta_{\mathrm{tot}} \end{aligned}\right\} \Rightarrow \theta = \frac{\theta_{\mathrm{tot}}}{1 + K_{\mathrm{G}}[\mathrm{G}]^h + [\mathrm{GRI}]/K_m} \tag{S11}$$

where θ_{tot} is the total number density of MR binding sites, $K_{\mathrm{G}} = k_3/k_{-3}$ is the glucose binding equilibrium constant, and $K_m = (k_2 + k_{-1})/k_1$ is the so-called Michaelis constant. The rate of GRI clearance via the MR route is therefore:

$$d[\mathrm{GRI}]/dt = k_2\theta_{\mathrm{GRI}} = \frac{k_2\theta_{\mathrm{tot}}[\mathrm{GRI}]}{K_m(1+K_{\mathrm{G}}[\mathrm{G}]^h)+[\mathrm{GRI}]} \quad \text{(S12)}$$

Apparently, if there is no glucose competing with MK-2640, $d[\mathrm{GRI}]/dt = k_2\theta_{\mathrm{tot}}[\mathrm{GRI}]/(K_m+[\mathrm{GRI}])$. The fractional inhibition by glucose, normalized by the uninhibited rate, is therefore:

$$\%\mathrm{Inhibition} = 1 - \frac{K_m+[\mathrm{GRI}]}{K_m(1+K_{\mathrm{G}}[\mathrm{G}]^h)+[\mathrm{GRI}]} \quad \text{(S13)}$$

The interplay between glucose and MK-2640 has been experimentally quantified by Kaarsholm *et al.* using a MR Biacore assay (S26). The assay, performed at a fixed MK-2640 concentration of 4 nM, suggested a K_m of approximately 3 nM. The remaining two unknowns, K_{G} and h, are then fitted to the experimental inhibition curve (Figure S3). With a K_{G} of 0.014 mM^{-h} and h of 2.537, the proposed MK-2640 kinetics matches the assay data almost perfectly. Furthermore, 2.537 is well within the typical range of 1 to 4 for Hill coefficients (S31). Our model inhibition curve translates to a half maximal inhibitory concentration (IC_{50}) of 7.5 mM, very close to the 8 mM reported in the article.

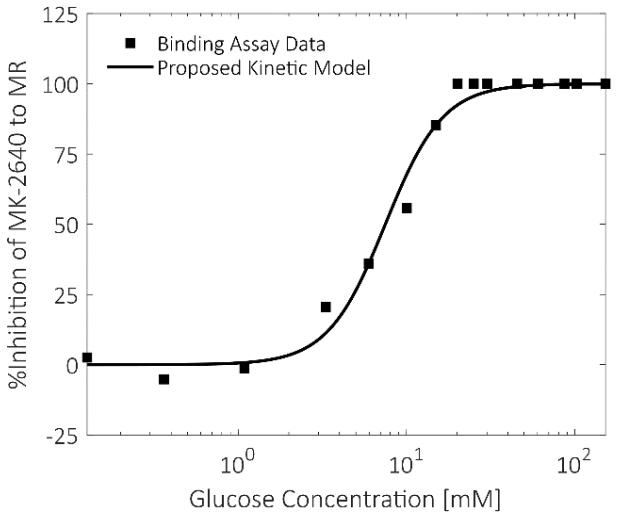

Figure S3. The proposed model (Equations S9 and S10) for MK-2640 kinetics fits the binding assay data almost perfectly. Data are digitized from Kaarsholm *et al.* (S26) with the bottom plateau shifted to 0.

With the MK-2640 chemical kinetics modeled, we will then plug Equation S12 back into the GRI kinetics terms of Equations S1 and S2, thereby interfacing the GRI action at the molecular level with the system-scale physiology. The generated ODE network from there will model how glucose and MK-2640 interact with the entire body. Naturally, the reports by the Merck team (S24,S26,S27,S33) on preclinical and clinical studies will provide valuable data for further model parameterization and refinement. We will then be able to gauge the translatability of the current MK-2640 formulation to the clinic following the same procedures detailed in the main text.

As in the freely circulating GRI case, the performance gap of MK-2640 may be a result of largely different anatomy and glucose metabolism between preclinical animals and humans. These distinctions aside, MK-2640's developers attributed the ineffective competitive clearance mechanism to MR saturation. As discussed in their clinical trial report (S24), "despite close cross-species homology for MRC1 structure,

incomplete understanding of quantitative differences across species in its CL [clearance] capacity complicate predictions of clinical GRI PK and CL", where "predictions" referred to using animals to replicate human conditions. Possible reasons for MR saturation in humans might be (i) insufficient MR availability, (ii) changed GRI or glucose binding affinity, or (iii) altered internalization (clearance) rate. These factors are respectively represented in the newly proposed kinetics (Equation S12) as $[\theta_{tot}]$, K_m, K_G, and k_2. MK-2640's binding constants K_m and K_G for animals and humans can be estimated from *in vitro* inhibition curves (S26) as already demonstrated in Figure S3. $[\theta_{tot}]$ and k_2 can be reversely inferred from GRI trial data (*e.g.* time courses of glucose level) if information is unavailable in the literature. The key is that, these parameters responsible for MK-2640's action profile likely assume (very) different values in animals and humans, thus contributing to the performance gap. This is how PAMERAH is capable of capturing the fundamental differences between humans and animals, even for complex GRIs like MK-2640.

Eventually, once PAMERAH indeed predicts MK-2640 as a false-positive (and hence to fail in humans) with its current kinetics, we will proceed to explore other regions of the parameter space and look for alternative designs promising adequate performances in both animals and humans. In summary, we outlined a plan for predicting MK-2640 performances with PAMERAH in this section, backed by preliminary results on modeling the competitive clearance kinetics. By applying PAMERAH to a commercially relevant GRI that met attrition at the clinical stage, this ongoing MK-2640 project will be a good demonstration on how model-aided rational design and translation can make a difference in the pharmaceutical community.

S4. Supplemental Figures

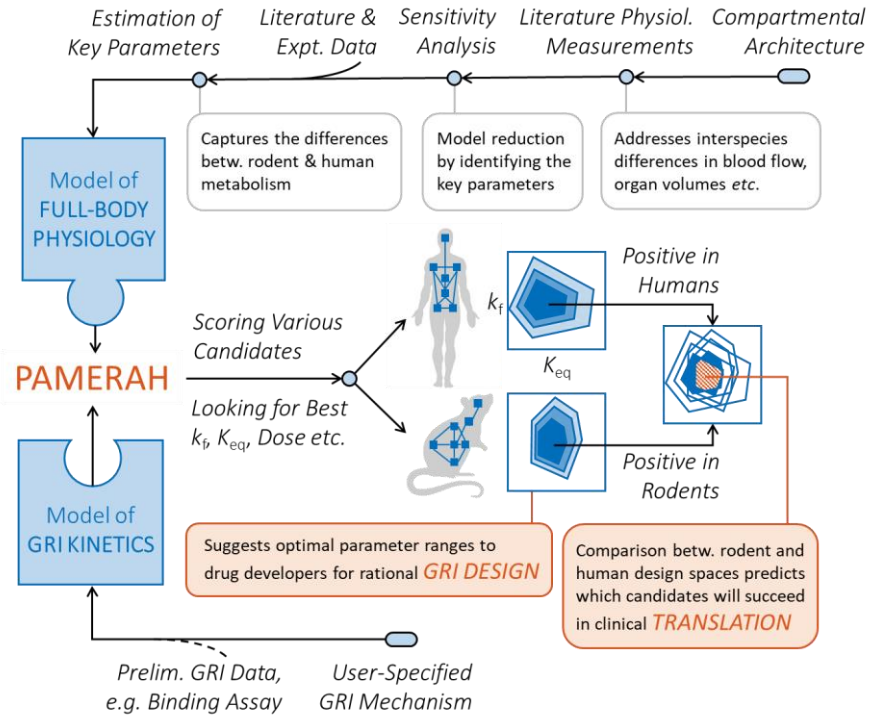

Figure S4. Schematic of the workflow of PAMERAH as well as its application to model-aided GRI design and translation. As described detailedly in the main text, PAMERAH was assembled by piecing together a set of user-specified GRI kinetics to a model for the full-body physiology. PAMERAH is able to explore a large design space, predicting performances of GRI constructs of arbitrary parameter combinations, such as k_f, K_{eq}, dose *etc*., thus aiding the rational design process. Furthermore, a cross-comparison between rodent and human design spaces identifies the optimal parameter ranges corresponding to adequate clinical translatability.

SUPPLEMENTARY DATA

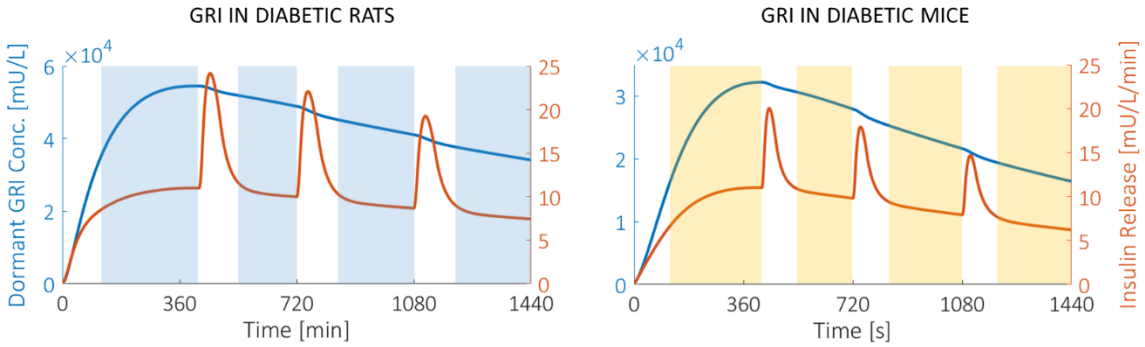

Figure S5. Time courses of the dormant GRI concentration (blue) and the insulin release rate (orange) simulated in average diabetic rats (left) and mice (right) respectively. They are the responses to a subcutaneous injection of a freely circulating GRI (k_f = 0.1 $M^{-1}min^{-1}$, K_{eq} = 0.02 M^{-1}, dosage = 300 μg/kg) at t = 0. The curves correspond to the glucose concentration trajectories presented in Figure 2 of the main article, and the shaded areas are identical to those in the said figure as well. Note that although the initial glucose concentrations are high in both diabetic rats and mice, we do not observe any initial spike in the insulin release rates. This is explained by the gradual absorption of GRI, as evidenced by the dormant GRI concentration curves.

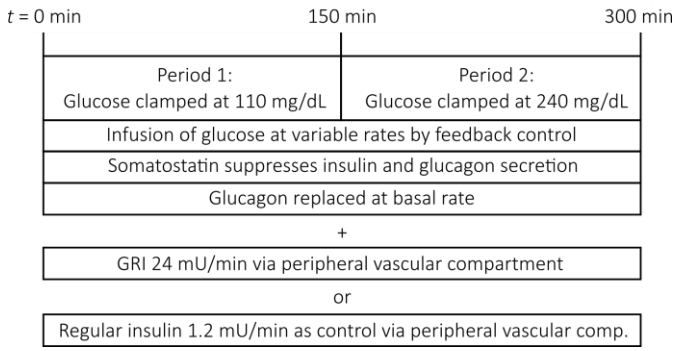

Figure S6. Protocol for the simulated pancreatic clamps corresponding to Figure 3 of the main article. Prior to the simulated clamp, PAMERAH assumes the state of a healthy rat. While in Moore *et al.*, the dog plasma glucose was clamped at 80 mg/dL during Period 1 (S27), the level is adjusted to 110 mg/DL for this simulation, within the typical range for rat clamps.

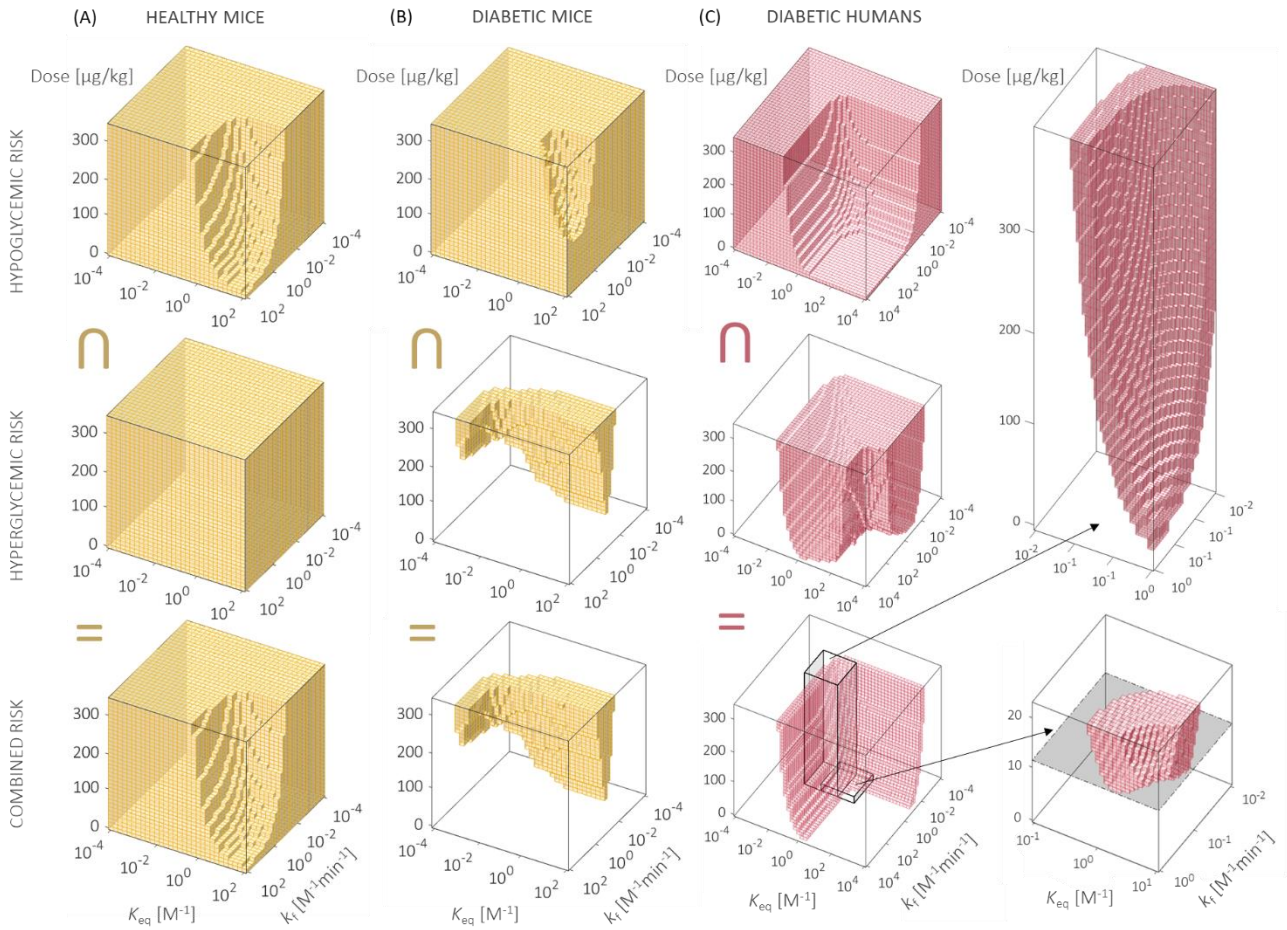

Figure S7. GRIDS and ODRs of (A) healthy mice, (B) diabetic mice, and (C) diabetic humans. The characteristic missing corner for healthy ODRs and *L* shape for the diabetic ODRs are observed in mice and humans as well. Parts of the human GRIDS are probed with refined resolutions, presented on the far right. The grey slice in panel (C) marks the predicted minimum effective dose for humans, 12.25 ± 0.25 µg/kg. Note that the bounds of human GRIDS are extended to accommodate a complete *L*-shaped cross-section. Only GRIDS for average diabetic humans is explored based on our previous work (S2).

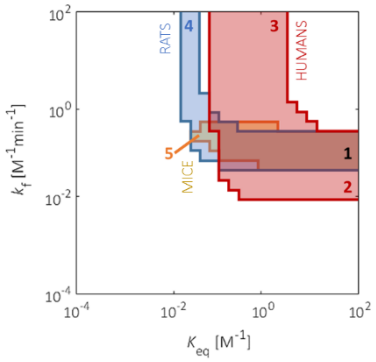

Figure S8. The translatability grid with a dosage range of 0 to 200 µg/kg, different from that in Figure 5. We see that the relative areas of true-positive (Zone 1), false-positive (Zones 4, 5), and false-negative (Zones 2, 3) regions are dependent on the bounds selected.

References

S1. Bisker G, Iverson NM, Ahn J, Strano MS. A pharmacokinetic model of a tissue implantable insulin sensor. Adv Healthc Mater. 2015;4(1):87–97.

S2. Bakh NA, Bisker G, Lee MA, Gong X, Strano MS. Rational design of glucose-responsive insulin using pharmacokinetic modeling. Adv Healthc Mater. 2017;6(22):1–10.

S3. Sorensen JT. A physiologic model of glucose metabolism in man and its use to design and assess improved insulin therapies for diabetes. Massachusetts Institute of Technology; 1985.

S4. Zhu JY, Dittmeyer R, Hofmann H. Application of sensitivity analysis to the reduction of a complex kinetic model for the homogeneous oxidative coupling of methane. Chem Eng Process. 1993;32(3):167–76.

S5. Dickinson RP, Gelinas RJ. Sensitivity analysis of ordinary differential equation systems-A direct method. J Comput Phys. 1976;21(2):123–43.

S6. Brown RP, Delp MD, Lindstedt SL, Rhomberg LR, Beliles RP. Physiological parameter values for physiologically based pharmacokinetic models. Toxicol Ind Health. 1997 Jul 30;13(4):407–84.

S7. Thurlby PL, Trayhurn P. Regional blood flow in genetically obese (ob/ob) mice. Pflügers Arch. 1980;385:193–201.

S8. Peters SA. Physiologically-Based Pharmacokinetic (PBPK) modeling and simulations: Principles, methods, and applications in the pharmaceutical industry. First Edit. Hoboken, New Jersey: John Wiley & Sons, Inc.; 2012.

S9. Ishise S, Pegram BL, Yamamoto J, Kitamura Y, Frohlich ED. Reference sample microsphere method: cardiac output and blood flows in conscious rat. Am J Physiol Circ Physiol. 1980 Oct;239(4):H443–H443.

S10. Wang P, Ba ZF, Burkhardt J, Chaudry IH. Trauma-hemorrhage and resuscitation in the mouse: effects on cardiac output and organ blood flow. Am J Physiol. 1993;264(4 Pt 2):H1166-73.

S11. Hutson NJ, Brumley FT, Assimacopoulos FD, Harper SC, Exton JH. Studies on the alpha-adrenergic activation of hepatic glucose output: I. Studies on the alpha-adrenergic activation of phosphorylase and gluconeogenesis and inactivation of glycogen synthase in isolated rat liver parenchymal cells. J Biol Chem. 1976 Sep 10;251(17):5200–8.

S12. Duca FA, Côté CD, Rasmussen BA, Zadeh-Tahmasebi M, Rutter GA, Filippi BM, et al. Metformin activates a duodenal Ampk-dependent pathway to lower hepatic glucose production in rats. Nat Med. 2015 Apr 6;21(5):506–11.

S13. Bachelard HS, Daniel PM, Love ER, Pratt OE. The transport of glucose into the brain of the rat in vivo. Proc R Soc B Biol Sci. 1973 Feb 27;183(1070):71–82.

S14. Goodman MN, Dluz SM, McElaney MA, Belur E, Ruderman NB. Glucose uptake and insulin sensitivity in rat muscle: Changes during 3-96 weeks of age. Am J Physiol Metab. 1983 Jan;244(1):E93–100.

S15. Robson AM, Srivastava PL, Bricker NS. The influence of saline loading on renal glucose reabsorption in the rat. J Clin Invest. 1968;47:329–35.

S16. Wong J, Chase JG, Hann CE, Shaw GM, Lotz TF, Lin J, et al. A subcutaneous insulin pharmacokinetic model for computer simulation in a diabetes decision support role: Model structure

and parameter identification. J Diabetes Sci Technol. 2008;2(4):658–71.

S17. Wong J, Chase JG, Hann CE, Shaw GM, Lotz TF, Lin J, et al. A subcutaneous insulin pharmacokinetic model for computer simulation in a diabetes decision support role: Validation and simulation. J Diabetes Sci Technol. 2008 Jul;2(4):672–80.

S18. Vogel S. Life's devices: The physical world of animals and plants. Princeton University Press; 1988.

S19. Tarín C, Teufel E, Picó J, Bondia J, Pfleiderer HJ. Comprehensive pharmacokinetic model of insulin glargine and other insulin formulations. IEEE Trans Biomed Eng. 2005;52(12):1994–2005.

S20. Jay TM, Jouvet M, Des Rosiers MH. Local cerebral glucose utilization in the free moving mouse: A comparison during two stages of the activity-rest cycle. Brain Res. 1985;342(2):297–306.

S21. Windmueller HG, Spaeth AE. Respiratory fuels and nitrogen metabolism in vivo in small intestine of fed rats: Quantitative importance of glutamine, glutamate, and aspartate. J Biol Chem. 1980 Jan 10;255(1):107–12.

S22. Özcan U, Yilmaz E, Özcan L, Furuhashi M, Vaillancourt E, Smith RO, et al. Chemical chaperones reduce ER stress and restore glucose homeostasis in a mouse model of type 2 diabetes. Science. 2006;

S23. Könner AC, Janoschek R, Plum L, Jordan SD, Rother E, Ma X, et al. Insulin action in AgRP-expressing neurons is required for suppression of hepatic glucose production. Cell Metab. 2007 Jun;5(6):438–49.

S24. Krug AW, Visser SAG, Tsai K, Kandala B, Fancourt C, Thornton B, et al. Clinical evaluation of MK-2640: An insulin analog with glucose-responsive properties. Clin Pharmacol Ther. 2019 Feb;105(2):417–25.

S25. Zion TC, Lancaster TC. Conjugate based systems for controlled drug delivery. WO2010088294, 2010.

S26. Kaarsholm NC, Lin S, Yan L, Kelly T, Van Heek M, Mu J, et al. Engineering glucose responsiveness into insulin. Diabetes. 2018;67(2):299–308.

S27. Moore MC, Kelley DE, Camacho RC, Zafian P, Ye T, Lin S, et al. Superior glycemic control with a glucose-responsive insulin analog: Hepatic and nonhepatic impacts. Diabetes. 2018;67(6):1173–81.

S28. Langmuir I. The adsorption of gases on plane surfaces of glass, mica and platinum. J Am Chem Soc. 1918 Sep;40(9):1361–403.

S29. Michaelis L, Menten ML. Die Kinetik der Invertinwirkung. Biochem Z. 1913;49:333–69.

S30. Berg JM, Tymoczko JT, Stryer L. Biochemistry. 5th ed. Biochemistry. New York, NY; 2002.

S31. Cortés A, Cascante M, Cárdenas ML, Cornish-Bowden A. Relationships between inhibition constants, inhibitor concentrations for 50% inhibition and types of inhibition: New ways of analysing data. Biochem J. 2001 Jul 1;357(1):263.

S32. Stefan MI, Le Novère N. Cooperative binding. Wodak S, editor. PLoS Comput Biol. 2013 Jun 27;9(6):e1003106.

S33. Yang R, Wu M, Lin S, Nargund RP, Li X, Kelly T, et al. A glucose-responsive insulin therapy protects animals against hypoglycemia. JCI Insight. 2018;3(1).